HAL
open science

Experimental Study of the Morphology of Two-phase Instabilities in Microgravity

Guillaume Renoux, Fabien Halter, Christian Chauveau

To cite this version:

Guillaume Renoux, Fabien Halter, Christian Chauveau. Experimental Study of the Morphology of Two-phase Instabilities in Microgravity. Atomization and Sprays, 2018, 28 (10), pp.915-929. 10.1615/AtomizSpr.2018028780 . hal-01955946

HAL Id: hal-01955946

https://hal.science/hal-01955946v1

Submitted on 16 Nov 2022

HAL is a multi-disciplinary open access archive for the deposit and dissemination of scientific research documents, whether they are published or not. The documents may come from teaching and research institutions in France or abroad, or from public or private research centers.

L'archive ouverte pluridisciplinaire **HAL**, est destinée au dépôt et à la diffusion de documents scientifiques de niveau recherche, publiés ou non, émanant des établissements d'enseignement et de recherche français ou étrangers, des laboratoires publics ou privés.

EXPERIMENTAL STUDY OF THE MORPHOLOGY OF TWO-PHASE FLAME INSTABILITIES IN MICROGRAVITY

G. Renoux, F. Halter, & C. Chauveau

CNRS - INSIS, Institut de Combustion, Aérothermique, Réactivité, Environnement, 1C Avenue de la Recherche Scientifique, 45100 Orléans, France

*Address all correspondence to: C. Chauveau, CNRS - INSIS, Institut de Combustion, Aérothermique, Réactivité, Environnement, 1C Avenue de la Recherche Scientifique, 45100 Orléans, France; Tel.: (+33) 238255486; Fax: (+33) 238696004, E-mail: christian.chauveau@cnrs-orleans.fr

This paper reports experimental studies of cellular flame instabilities in the case of an expanding two-phase spherical flame under microgravity conditions. The presence ofliquid fuel droplets leads to the triggering of those instabilities on the flame surface (cracks or cellular) which have an extensive impact on flame behavior, such as propagation speed and morphology. The main focus is to figure out the interaction of the droplets with the propagating flame. A high-speed shadowgraphy technique is used along with a specific segmentation posttreatment to obtain quantitative access to the flame propagation and morphology. In a second time, CH* chemiluminescence is used concurrently with high-speed interferometric laser imaging for droplet sizing or planar Mie scattering for a simultaneous characterization of the flame structure and aerosol properties. By a comparison with equivalent gaseous flames, the impact of the two-phase configuration is assessed. In addition, this study proposes a quantitative analysis of the cell size distribution over the flame propagation. It is finally shown that the size of the cells is not directly correlated with the droplet interdistance, which indicates that the droplets only act as a trigger for the development of the instabilities.

KEYWORDS: aerosol flame, two-phase combustion, cellular instabilities, cellular wavelength, flame morphology

1. INTRODUCTION

Spray combustion is widely used in practical applications of energy conversion such as rocket, turbofan, and diesel engines as well as industrial furnaces. The presence of droplets in the mixture has a large impact on the combustion process and introduces many complex phenomena, such as vaporization, fluid dynamics, and heterogeneous combustion. It is well known that the flame propagation speed may be dramatically enhanced in two-phase combustion (Atzler, 1999; Nomura et al., 1998). Indeed, it is currently admitted that this phenomenon is related to the increase of the flame area due to the wrinkling caused by instabilities on the flame surface (Hayashi et al., 1977). Moreover, it has been demonstrated (Lawes et al., 2002) that aerosol flames become unstable earlier than gaseous flames. This result has also been confirmed for ethanol two-phase flames (Thimothée et al., 2015). It has been suggested that the main phenomenon causing the

The publisher version is available using this link :

please cite using the following format :
Renoux G, Halter F, Chauveau C. EXPERIMENTAL STUDY OF THE MORPHOLOGY OF TWO-PHASE FLAME INSTABILITIES IN MICROGRAVITY. 2018;28:915-29. 10.1615/AtomizSpr.2018028780.

instability in two-phase combustion is the fact that droplets may act as obstacles to the propagation of the flame (Thimothée et al., 2016), as they create a locally high gradient of fuel concentration while evaporating. This phenomenon is then directly correlated with the topology of the instabilities (Thimothée, 2017; Thimothée et al., 2017).

It is necessary to predict both the onset and development of instabilities for two-phase mixture combustion, as a faster burning rate is either an advantage, such as for engines, or a hazard in an industrial context. This study offers a quantitative experimental investigation of the morphology of unstable two-phase flames. The link between the flame morphology and the properties of fuel aerosol is also investigated. In addition, the pertinence of the use of shadowgraphy in quantitative instability studies is assessed by comparing its results with those of CH* chemiluminescence method.

2. EXPERIMENTAL METHODS

Experiments are conducted in a pressure-release-type dual chamber which is adequate for aircraft-related safety requirements (cf. Fig. 1). It consists of a 1 L spherical combustion chamber which is inserted in an 11 L high-pressure chamber. The inner and the outer chambers are filled simultaneously with the flammable mixture and nitrogen, respectively. The flammable mixture is composed of gaseous ethanol diluted in synthetic air (80% N_2, 20% O_2).

The fuel aerosol is generated by the Wilson cloud chamber method (Wilson, 1951). The inner chamber is connected by a valve to a 2.5 L expansion vessel which is initially vacuumed. The opening of the valve induces a pressure drop in the combustion chamber, which induces a temperature drop. When the partial pressure of ethanol becomes greater than the saturation pressure, it starts to condense into a cloud of droplets. The mixture is finally ignited at the center of the vessel by using two tungsten electrodes. The granulometry of the aerosol (droplet size and interdistance) is controlled by the thermodynamic parameters of the experiment: the initial

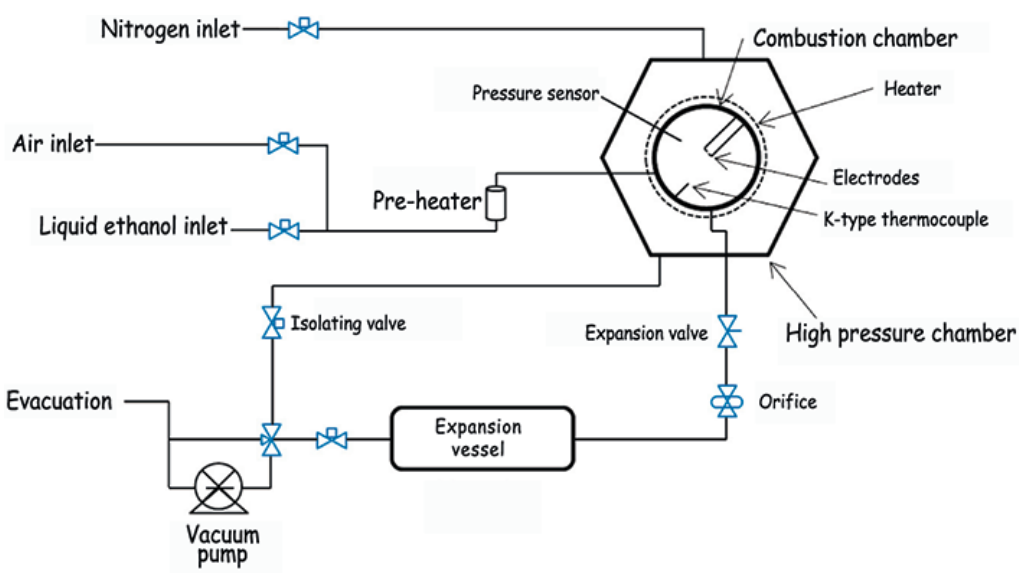

FIG. 1: Schematic representation of the experimental apparatus

pressure P_i, the total equivalence ratio φ, the pressure drop ΔP, and the pressure drop duration t_{fall}.

Eight evacuation valves are placed around the combustion chamber to release the pressure into the high-pressure chamber during the combustion. As the volume ratio between the outer and inner chambers is 10:1, the pressure rise is greatly reduced. In addition, the dilution in nitrogen ensures the nonpropagation of the flame in the outer chamber.

Experiments conducted in terrestrial gravity are characterized by the sedimentation of the droplets. Indeed, the fall of the droplets at their terminal velocity, which depends on the droplet radius, causes their stratification in the combustion chamber. In order to avoid this effect, experiments are carried out under microgravity conditions obtained during parabolic flights on board the National Center for Space Studies Airbus A310 ZERO-G. Periods of 22 s of weightlessness condition under 10^{-2} g are achieved during those flights.

Both chambers are equipped with aligned transparent windows to allow optical access. In addition, a laser device (Coherent Verdi) emitting at 532 nm is used to create a thin laser sheet at the center of the combustion chamber. Two diagnostics are used to characterize the aerosol prior to ignition. First, planar Mie scattering is employed to have access to the position, to the interdistance distribution a of the droplets, and to the mean interdistance a_{mean}. A high-speed camera (Phantom v1210) is focused on the laser sheet and receives the light scattered by the fuel droplets (Fig. 2).

Second, droplet size is evaluated by the interferometric laser imaging for droplet sizing (ILIDS) technique. By defocusing the camera (Phantom v1210), an interference fringe pattern is obtained for each droplet present inside the laser sheet (Fig. 3). The number of fringes on the pattern is proportional to the geometrical diameter of the droplet, with a coefficient depending on the geometry of the system [Eq. (1)] (Lemaitre et al., 2007; Mounaim-Rousselle and Pajot, 1999).

$$d_{droplet} = N_{fringe} \times \frac{2\lambda}{\alpha}\left(\cos(\theta/2) + \frac{m\sin(\theta/2)}{\sqrt{m^2 - 2m\cos(\theta/2) + 1}}\right)^{-1} \quad (1)$$

with $d_{droplet}$ the droplet diameter, N_{fringe} the number of fringe on the image, θ the scattering angle (here 90°), α the collecting angle, λ the laser wavelength, and m the refractive index of the

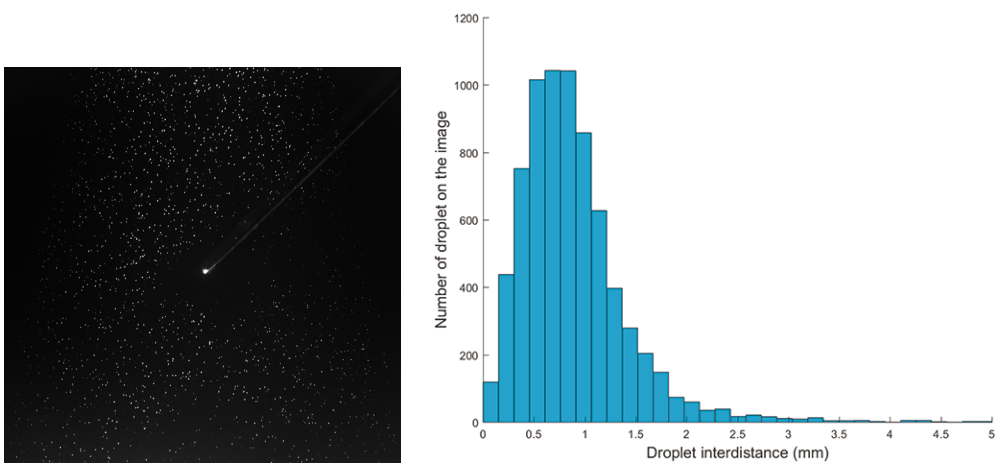

FIG. 2: Planar Mie scattering raw image and extracted droplet interdistance distribution

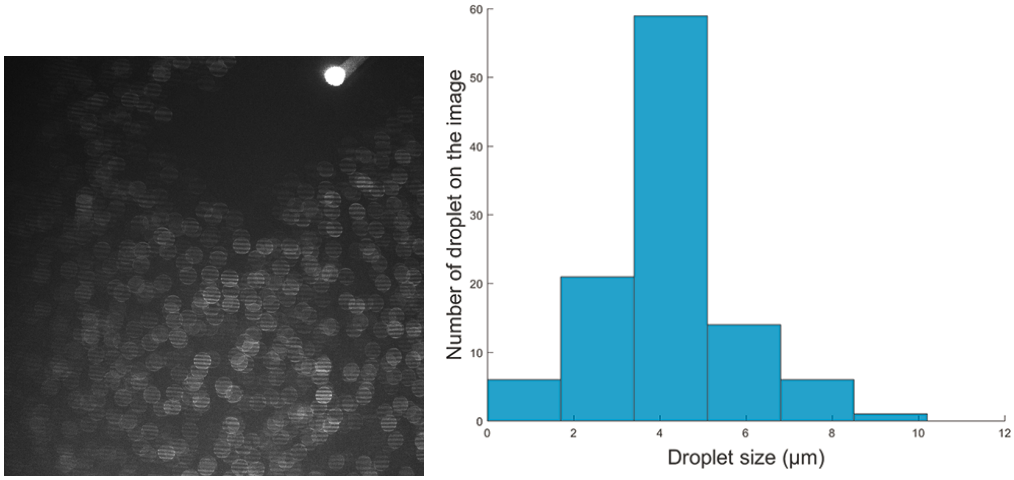

FIG. 3: ILIDS raw image and extracted droplet size distribution

liquid. With the setup used, the obtained resolution is 1.8 µm/fringe. For dense aerosols, some overlapping of the fringe patterns can be observed on the images. However, it is assumed that the droplet size distribution is not affected by this effect. Indeed, the diameter of the circular patterns is only dependent on the optical setup and not on the droplet size. Moreover, this method is not used to compute the aerosol droplet density, for which fringe pattern overlapping could have a large impact.

The combustion is monitored by several diagnostics. First, a shadowgraphy system is used to visualize the time evolution of the morphology of the flame surface, as the instabilities appear luminous in the same way as the flame front. The flame is back-illuminated thanks to a laser-driven light source (Energetiq LDLS) and its time evolution is recorded by a high-speed camera (Phantom v1611). As this method requires two optical accesses, it cannot be simultaneously used with another diagnostic.

The second diagnostic is the chemiluminescence visualization of the flame (Bradley et al., 2000). In contrast to the shadow method, this technique uses the light emission produced by the flame. The CH* radical is a reliable tracker of the flame reaction zone and emits light at 430 nm. The continuous emission spectrum of the flame is filtered with an interference filter in order to uphold only this wavelength (Kojima et al., 2000). The intensity of the light once filtered is particularly low, therefore a light intensifier (LaVision High-Speed IRO) is coupled to the high-speed camera (Phantom v1611). The depth of field of the optical system is relatively narrow (i.e., 1 cm). Thus, by focusing the camera on the forward hemisphere, it is certain that all the morphology seen is located at its surface because the details of the other hemisphere will be blurred on the image. Because of configuration constrains, the setup can use the following combination of simultaneous optical diagnostics:

- chemiluminescence + planar Mie scattering
- chemiluminescence + ILIDS
- planar Mie scattering + ILIDS
- shadowgraphy

More details about the experimental apparatus and the diagnostic setup can be found in previous publications (Thimothée, 2017; Thimothée et al., 2016).

3. IMAGE POSTPROCESSING

In order to study the morphology of unstable flames, cells present on the flame surface must be identified and segmented on raw shadowgraphy images (Fig. 4). The specific postprocessing of those images consists of the following sequence:

1. *Image processing and segmentation.* A top-hat filter is used to highlight ridges on the image. Then, an anisotropic nonlinear Perona-Malik diffusion (Perona and Malik, 1990) cleans the image. Next, an H-minima transform removes the smallest and nonsignificant local minima. The cell population is finally segmented by a watershed algorithm (Meyer, 1994).
2. *Tracking.* The watershed algorithm returns the cells in an arbitrary order. Thus, individual cells must be tracked between images in order to follow their evolution over time. The selected algorithm uses a method based on a metric optimization. This metric is based on the overlap of the cells between two images, on the distance between their centroid, and on the difference of their size (Chalfoun et al., 2009).
3. *Projection correction.* By recording the flame on the camera sensor, the flame is projected from a three-dimensional geometry to a two-dimensional plane. Therefore, the geometrical information measured on the image must be corrected. However, as the amplitude of the cells is small and cannot be measured experimentally with our setup, it is then assumed that the flame is spherical. The surface element is corrected as follows, with r being the distance from the center of the flame and the element on the recorded image and R_f being the radius of the flame.

$$dS_{real} = \frac{1}{\sqrt{1 - r^2/R_f^2}} dS_{recorded} \tag{2}$$

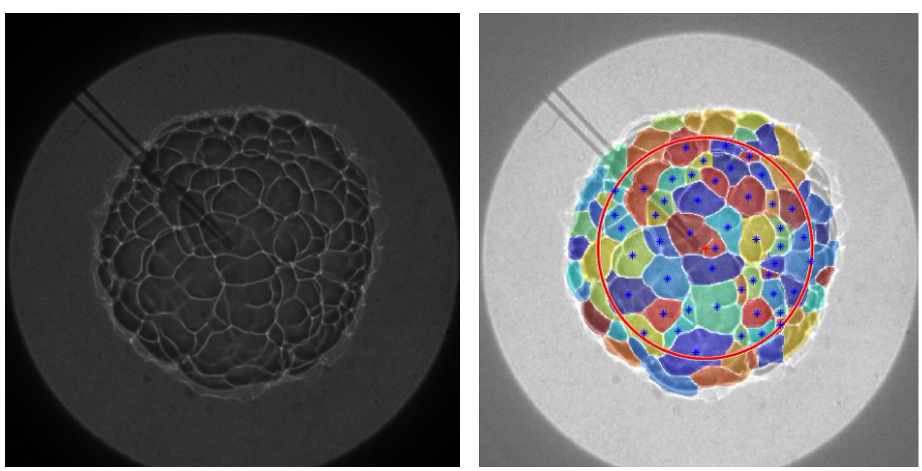

FIG. 4: Raw and fully segmented shadowgraphy image

The characteristic distances are recalculated by the Haversine formula, with Φ and λ being, respectively, the latitude and the longitude (Sinnott, 1984).

$$\Delta d = 2R_f \arcsin \sqrt{\sin^2 \frac{\Delta\Phi}{2} + \cos\Phi_1 \cos\Phi_2 \sin^2 \frac{\Delta\lambda}{2}} \tag{3}$$

4. COMPARISON OF SHADOWGRAPHY AND CHEMILUMINESCENCE

In order to be consistent with other studies, this paper uses the notation used by the linear modelling of gaseous flame instabilities (Addabbo et al., 2002; Bechtold and Matalon, 1987). The flame size is described by a dimensionless Peclet number [Eq. (4)], given by the ratio of the flame radius R_{flame} to its thickness δ_L. The flame thickness is calculated numerically for a premixed unstretched 1D flame with a detailed chemical model (Leplat et al., 2011) and with the thermal thickness definition (Poinsot and Veynante, 2005; Spalding, 1955)

$$\mathrm{Pe} = \frac{R_{flame}}{\delta_L}, \quad \delta_L = \frac{T_{burn} - T_{unburn}}{(dT/dx)_{max}} \tag{4}$$

The size of the instability cells is described by a dimensionless wavenumber given by the ratio of the flame perimeter to the wavelength of the cell (Beeckmann et al., 2017). The equivalent major axis a_{cell} is chosen as the experimental value of the wavelength [Eq. (5)]. Thus, the small cells have a high wavenumber and the large cells a small one.

$$n = \frac{L_{flame}}{L_{cell}} = \frac{2\pi R_{flame}}{a_{cell}} \tag{5}$$

The linear stability analysis describes the onset and the development of cellular instabilities. The growing rate of a disturbance of wavenumber n on the surface of a spherical expanding flame is described by

$$\begin{gathered} \frac{1}{A}\frac{dA}{dt} = \frac{\dot{R}}{R}\left(\omega - \frac{\delta_L}{R}\Omega\right) \\ \Omega = \Omega_1 + \left(\mathrm{Ze}\frac{\mathrm{Le}_{eff} - 1}{\sigma - 1}\right)\Omega_2 + \mathrm{Pr}\,\Omega_3 \end{gathered} \tag{6}$$

where A is the amplitude of the instability, ω a coefficient corresponding to Darrieus-Landau (hydrodynamic) instability, Ze the Zeldovich number, Le_{eff} the effective Lewis number, $\sigma = T_b/T_u$ the thermal expansion ratio, and Pr the Prandtl number. Ω_1, Ω_2, and Ω_3 correspond, respectively, to thermal, molecular, and viscous diffusions. Both ω and Ω depend only on n, σ, and on a profile of the thermal conductivity through the flame.

The onset of instability can occur only if the growth rate of at least a wavenumber is positive. Therefore, all stable cells are characterized by

$$\frac{\omega(n)}{\Omega(n)} > \mathrm{Pe} \tag{7}$$

This analysis produces stability curves as shown in Fig. 5, with the reasonable assumption that for the thermal conductivity $\lambda \propto T^{1/2}$ (Beeckmann et al., 2017). The dot-dashed line represents the boundary between stable (on the left) and unstable flames (on the right). The leftmost

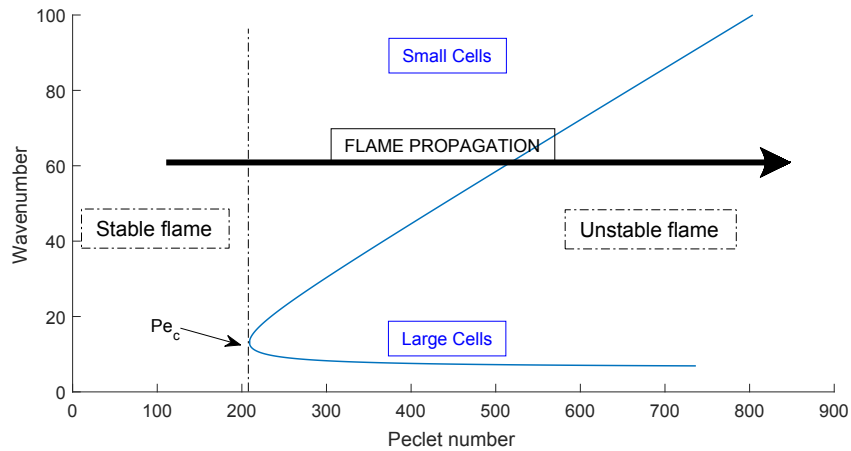

FIG. 5: Peninsula of unstable modes for a gaseous equivalent to condition 3 (P_{igni} = 0.33 MPa, φ = 1.4)

point on the stability curve corresponds to the onset of instability and is characterized by its critical Peclet number Pe_c. All cells present on the unstable flame surface are located on the right of the stability curve, with the smallest cells being toward the upper branch of the curve and the biggest toward the lower branch.

Table 1 exhibits the experimental conditions used for this study, numbered from 1 to 6. The computed physical parameters used to compute the linear stability analysis are also explicit.

Shadowgraphy and chemiluminescence differ in a fundamental way (cf. Fig. 6). Shadowgraphy is sensitive to the second derivative of the gas refractive index m, so to the second derivative of the temperature as $m \propto T$ for an ideal gas. The CH* chemiluminescence is sensitive to the emission created by the deexcitation of the CH* radical in the reaction zone. In our case, we take advantage of the fact that this signal is notably affected by the local curvature of the flame. The boundary between cells being highly negatively curved, chemiluminescence is a good indicator of the flame morphology. In addition, for the shadowgraphy, the light emitted by the light source is deviated by each flame front, so twice. This may introduce a superposition or at least a distortion of the instability pattern.

TABLE 1: Experimental conditions and parameters used during this study. Flame parameters are calculated numerically with the Leplat mechanism

Condition	P_{igni} (MPa)	φ	ΔP (MPa)	T_{igni} (K)	a_{mean} (mm)	*SMD* (μm)	δ_L (mm)	$\sigma_{thermal}$	Ze	Le_{eff}	Pr
1	0.25	1.2	0.15	337	0.527 ± 0.05	9.8 ± 0.9	0.21	7.0	7.833	1.12	0.76
2	0.33	1.3	0.12	341	0.596 ± 0.05	8.3 ± 0.9	0.19	6.9	9.187	1.10	0.76
3	0.33	1.4	0.12	341	0.538 ± 0.05	8.7 ± 0.9	0.24	6.8	11.03	1.04	0.77
4	0.30	1.1	0.20	339	0.497 ± 0.05	9.9 ± 0.9	0.18	7.1	7.118	1.19	0.76
5	0.30	1.2	0.20	339	0.502 ± 0.05	9.9 ± 0.9	0.21	6.9	9.798	1.08	0.76
6	0.34	1.0	0.25	335	0.468 ± 0.05	9.6 ± 0.9	0.18	7.1	9.092	1.31	0.75

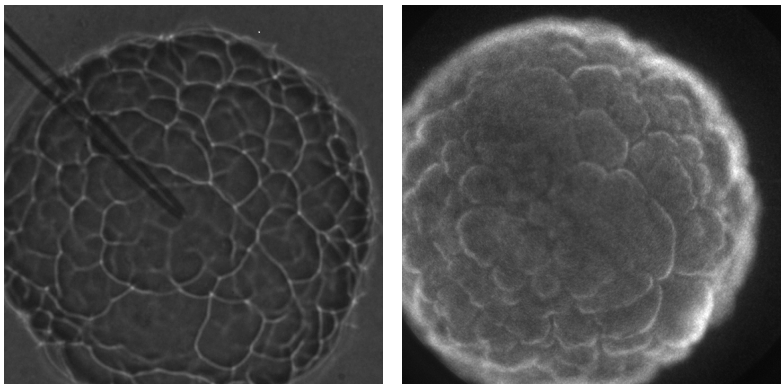

FIG. 6: Comparison of (left) shadowgraphy and (right) CH* chemiluminescence for two equivalent flames and at a radius of 13.5 mm (P_{igni} = 0.25 MPa, φ = 1.2, ΔP = 0.15 MPa)

To evaluate this, we use the CH* chemiluminescence as the reference, the light emitted by the flame being influenced only by the flame front which emitted it.

Figure 7 compares the results of the segmentation for two different mixtures at an equivalence ratio of 1.3 (a) and 1.4 (b). For clarity, only the envelope of the cell population is shown. In order to have a statistically meaningful database, each condition has been repeated five times for shadowgraphy (dots) and 10 times for chemiluminescence (stars). From shadowgraphy measurements, the black dashed lines show the ± 2 standard deviation of the mean of the maximal wavenumber. As its distribution is unimodal, the Vysochanskii-Petunin inequality (Pukelsheim, 1994) states that at least 89% of the wavenumbers should be located between these lines. However, only 31% (a) and 25% (b) of the cells detected by CH* chemiluminescence are within those bounds. Therefore, it is shown that this cells detection by shadowgraphy overestimates the minimal size of the cells. However, the sizes of the largest cells are similar between these two methods.

The superposition on shadowgraphy images has an impact on the measured distributions of cell size, as presented in Fig. 8 for two particular Peclet numbers. As observed before, the

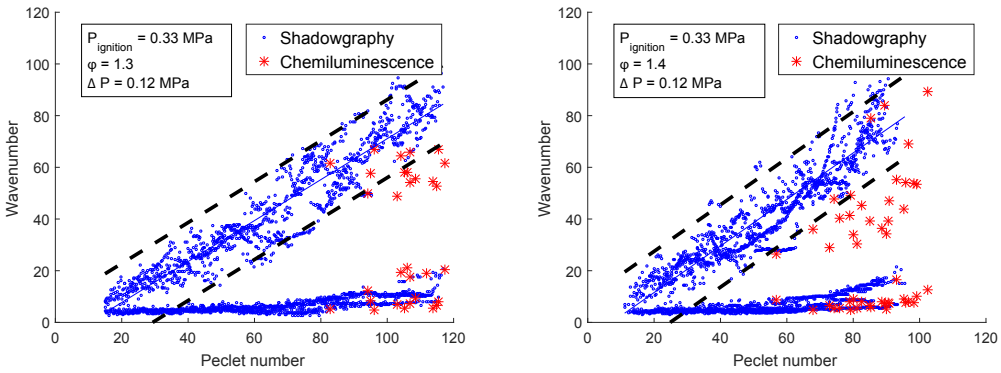

FIG. 7: Comparison of the envelope of the cell size distribution between (dots) shadowgraphy and (stars) CH* chemiluminescence for conditions 2 and 3

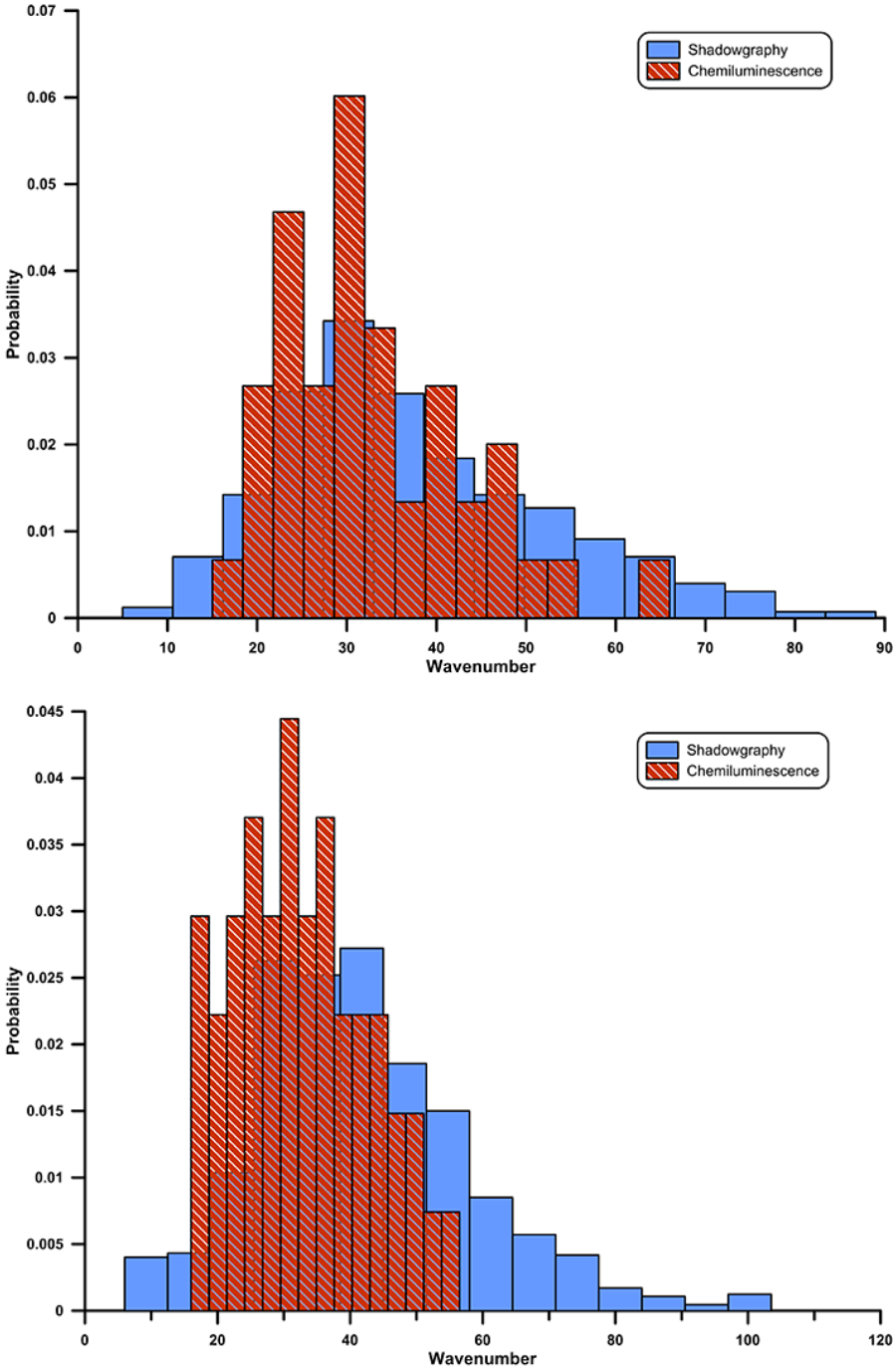

FIG. 8: Comparison of the cell size distribution between shadowgraphy and CH* chemiluminescence for conditions 2 and 3 at Pe = 107 and 93, respectively

envelopes obtained by chemiluminescence are sharper than those obtained by shadowgraphy. However, the peak of the distribution seems to be similar between those methods.

5. AEROSOL FLAME INSTABILITY

As stated earlier (Bradley et al., 2014), the presence of fuel droplets in the mixture has a large impact on the stability of the flame. Figure 9 illustrates the difference between two-phase flames and the linear model of their gaseous equivalent. The temperature differs between experiments due to the variation of pressure drop used to condense the ethanol. However, the initial temperature prior to ignition has a negligible impact on the critical Peclet number (Sun et al., 2012).

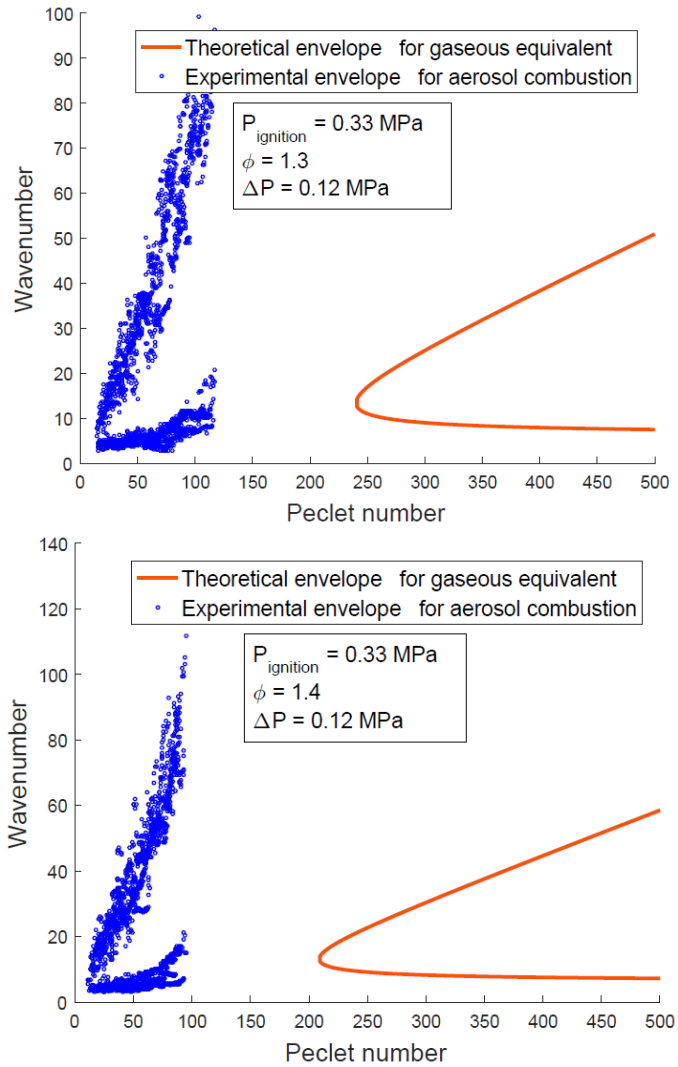

FIG. 9: Comparison of instability wavenumber envelope for experimental two-phase flame and its gaseous theoretical equivalent for conditions 2 and 3

Both two-phase and gaseous unstable flames exhibit the same trend. Indeed, the instability region is similarly contained in a peninsula with a linear trend over high wavenumbers and with a nearly constant pattern for low wavenumbers. In terms of cell size, the largest cells tend to have a constant size in units of flame perimeter while the smallest cells are increasingly smaller when the flame propagates.

Two main dissimilarities appear. First, and as expected from literature, the critical Peclet number is much smaller for two-phase flames than for gaseous flames. It corresponds to an earlier apparition of instabilities during the flame propagation. Second, the slope of the maximal wavenumber is higher for two-phase flames. It means that smaller cells appear earlier after the onset of instabilities compared to the linear model, the slope being increased by a factor between 5.6 and 7.0 in our experimental conditions. However, it should be noted that, according to Matalon (2005), this model drastically underestimates the slope of those high wavenumbers but estimates correctly the critical Peclet number. Another study (Law et al., 2005) has confirmed a correct evaluation of the critical Peclet number by the linear model for hydrogen flames. Thus, a peculiar attention has to be paid while interpreting the slope modification for high wavenumbers.

It is interesting to note that the model used to describe the instability peninsula for gaseous flames (Addabbo et al., 2002) cannot be directly fitted to the two-phase experimental data by varying the parameters σ, Le_{eff} , Ze, and Pr. This indicates that the presence of droplets in the mixture does not only vary the physical parameters but also modifies the physics of the combustion.

Figure 10 shows the distribution of cell wavenumbers during the flame propagation. The boundaries of the peninsula correspond to the curves previously shown in Fig. 9. For a constant Peclet number, the cell wavenumber distribution is asymmetric and positively skewed (positive third normalized moment). The skewness varies between 0.5 and 1.2. Therefore, the mode of the population, i.e., its most representative size, is located toward the lower wavenumbers (larger cells).

The location of this mode can be approximated by Eq. (8) in the (Pe, n) space.

$$\mathrm{mode}(n_{cell}) = \max(n_{cell}) = \gamma_1(Pe - Pe_c)^{\gamma_2} + n_c \tag{8}$$

Table 2 shows the result obtained by fitting Eq. 8 to our experimental data. The exponent γ_2 varies widely from 0.6 to 2.2 in the experimental conditions. This implies a wide behavior for the characteristic size of the cell. It may either stay close to the largest cells ($\gamma_2 < 1$) or move toward the smallest cells ($\gamma_2 > 1$).

It should also be noted that the wavenumbers corresponding to the droplet interdistance $n_{droplet} = 2\pi R_{flame} / a_{droplet}$ are 2–5 times higher than maximal wavenumbers and 8–15 times higher than the mode wavenumbers. It indicates that the droplets only act as a trigger to the development of the instabilities. The development of the instability is then driven by the intrinsic gaseous instability of the flame (hydrodynamic and thermodiffusive instabilities). This confirms the results obtained in previous studies (Nicoli et al., 2017; Thimothée, 2017). In practice, for aerosol combustion, the droplet interdistance has an obvious effect on the flame morphology [Fig. IV.6 in Nassouri (2014)]; however, this phenomenon might be caused by the continuous triggering of the instabilities by the cloud of droplets.

The development of each individual cell can be monitored during the propagation of the flame. In order to track the evolution of each individual cell surface over time and regarding of its size, we define a surface increase rate per unit of surface. This definition corresponds to $K_A = 1/A_{cell}\ dA_{cell}/dt$, which coincides with the stretch of the cell surface.

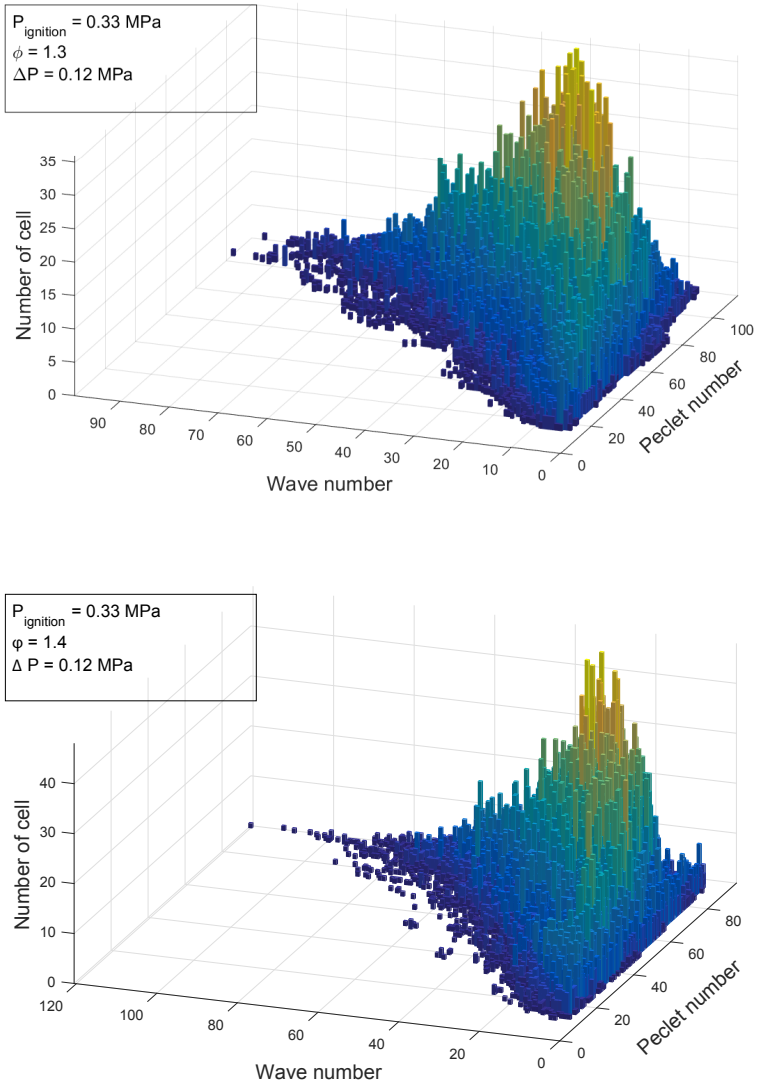

FIG. 10: Distribution of cell wavenumbers during the flame propagation

Figure 11 shows the evolution of the cell stretch during the flame propagation. Some negative values are not shown in the figure due to the semilog scale and correspond to the split of some cells during the flame propagation. The cell stretch distribution is spread out over a wide range of values. It indicates that the cell growth is highly variable within the population. However, there is no direct relationship between the cell size and its stretch. Indeed, the correlation coefficient between those values is no higher than 0.08 for the present experimental conditions. It may indicate that the growth speed is either chaotic or dependent on other parameters, such as the neighboring cells or the amplitude of the instability.

TABLE 2: Results of the fit of Eq. (8) for the mode of the cell size distribution

Condition	γ_1	γ_2	n_c	Pe_c	Fit r^2
1	0.17	1.1	1.7	13	0.95
2	0.019	1.6	2.4	14	0.92
3	0.0012	2.2	3.9	11	0.90
4	0.32	0.88	2.1	16	0.69
5	0.55	0.89	1.5	13	0.92
6	1.3	0.58	0.95	16	0.74

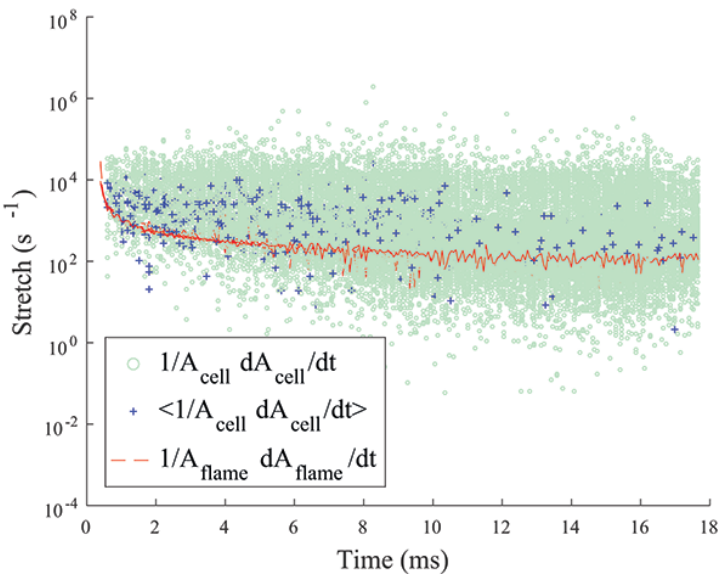

FIG. 11: Evolution of flame and cell stretch during the propagation of the flame for the condition 2

6. CONCLUSION

This work takes place in the framework of the experimental study of the interaction between flames and fuel aerosols. The developed experimental apparatus focuses on two-phase spherical expanding flames and relies on high-speed optical diagnostics. It has been previously shown that the flame speed and the flame stability can be dramatically modified for a two-phase flame, in comparison to an equivalent gaseous flame. In addition, it was demonstrated that this instability enhancement is caused by the high local gradient of density of equivalence ratio.

In this study, the morphology of unstable ethanol two-phase flame has been described and quantified experimentally by CH* chemiluminescence and shadowgraphy. In addition, the differences between those methods have been assessed. It has been shown that those two diagnostics do not produce the same result on the bounduaries of the cell size distribution, especially for the small cells. However, the peak of the distribution is similar for the two diagnostics. In addition, by a comparison with a linear model of unstable gaseous flames, it has been demonstrated that

the presence of fuel droplets in the mixtures has a large impact on the flame morphology. Indeed, they induce an earlier triggering of the instabilities and tend to modify the distribution of cell size at the flame surface. Moreover, the characteristic size of the cells can be represented by a power law in the (Pe, n) space. However, the growth rate of each individual cell is heavily scattered and is not related to the cell size. Finally, the cell size is not directly correlated with the droplet interdistance. This indicates that the droplets act only as a trigger for the development of the instabilities, which are then driven by the intrinsic gaseous flame instabilities.

ACKNOWLEDGMENTS

We acknowledge the CNES for its financial support. We are also thankful to the Région Centre Val de Loire and the French Government Program "Investissements d'avenir" through the LABEX CAPRYSSES ANR-11-LABX-0006-01.

REFERENCES

Addabbo, R., Bechtold, J., and Matalon, M., Wrinkling of Spherically Expanding Flames, *Proc. Combust. Inst.*, vol. **29**, no. 2, pp. 1527–1535, 2002.

Atzler, F., Fundamental Studies of Aerosol Combustion, PhD, University of Leeds, West Yorkshire, England, 1999.

Bechtold, J.K. and Matalon, M., Hydrodynamic and Diffusion Effects on the Stability of Spherically Expanding Flames, *Combust. Flame*, vol. **67**, no. 1, pp. 77–90, 1987.

Beeckmann, J., Hesse, R., Kruse, S., Berens, A., Peters, N., Pitsch, H., and Matalon, M., Propagation Speed and Stability of Spherically Expanding Hydrogen/Air Flames: Experimental Study and Asymptotics, *Proc. Combust. Inst.*, vol. **36**, no. 1, pp. 1531–1538, 2017.

Bradley, D., Lawes, M., Liao, S., and Saat, A., Laminar Mass Burning and Entrainment Velocities and Flame Instabilities of I-Octane, Ethanol and Hydrous Ethanol/Air Aerosols, *Combust. Flame*, vol. **161**, no. 6, pp. 1620–1632, 2014.

Bradley, D., Sheppart, C.G., Woolley, R., Greenhalgh, D.A., and Lockett, R.D., The Development and Structure of Flame Instabilities and Cellularity at Low Markstein Numbers in Explosions, *Combust. Flame*, vol. **122**, nos. 1-2, pp. 195–209, 2000.

Chalfoun, J., Cardone, A., Dima, A.A., Allen, D.P., and Halter, M.W., Overlap-based Cell Tracker, *J. Res. Nat. Inst. Stand. Technol.*, vol. **115**, no. 6, p. 477, 2009.

Hayashi, S., Kumagai, S., and Sakai, T., Propagation Velocity and Structure of Flames in Droplet-Vapor-Air Mixtures, *Combust. Sci. Technol.*, vol. **15**, nos. 5-6, pp. 169–177, 1977.

Kojima, J., Ikeda, Y., and Nakajima, T., Spatially Resolved Measurement of OH*, CH *, and C* Chemiluminescence in the Reaction Zone of Laminar Methane/Air Premixed Flames, *Proc. Combust. Inst.*, vol. **28**, pp. 1757–1764, 2000.

Law, C.K., Jomaas, G., and Bechtold, J.K., Cellular Instabilities of Expanding Hydrogen/Propane Spherical Flames at Elevated Pressures: Theory and Experiment, *Proc. Combust. Inst.*, vol. **30**, no. 1, pp. 159–166, 2005.

Lawes, M., Lee, Y., and Marquez, N., Enhanced Burning Rates due to Droplet Induced Flame Instabilities, *Proc. of the 18th European Conf. on Liquid Atomization and Spray Systems*, Zaragoza, Spain, Sept. 9–11, 2002.

Lemaitre, P., Porcheron, E., Nuboer, A., and Gréhan, G., Interferometric Laser Imaging Development for Droplets Sizing (ILIDS) in Hostile Environment, *Proc. of the 10th Intl. Conf. on Liquid Atomization and Spray Systems*, 2007.

Leplat, N., Dagaut, P., Togbé, C., and Vandooren, J., Numerical and Experimental Study of Ethanol Combustion and Oxidation in Laminar Premixed Flames and in Jet-Stirred Reactor, *Combust. Flame*, vol. **158**, no. 4, pp. 705–725, 2011.

Matalon, M., The Development of Hydrodynamically Unstable Flames, *The 20th Intl. Collegium Dynamics Expositions and Reactive Systems*, pp. 1–5, McGill University, Montreal, Canada, July 31 – Aug. 5, 2005.

Meyer, F., Topographic Distance and Watershed Lines, *Signal Process.*, vol. **38**, no. 1, pp. 113–125, 1994.

Mounaim-Rousselle, C. and Pajot, O., Droplet Sizing by Mie Scattering Interferometry in a Spark Ignition Engine, *Part. Part. Syst. Charact.*, vol. **16**, no. 4, pp. 160–168, 1999.

Nassouri, M., Caractérisation Expérimentale de la Propagation d'une Flamme Laminaire dans un Milieu Diphasique (Brouillard) à Haute Pression et en Microgravité, PhD, Autre Université d'Orléans, France, 2014.

Nicoli, C., Haldenwang, P., and Denet, B., Darrieus-Landau Instability of Premixed Flames Enhanced by Fuel Droplets, *Combust. Theor. Modell.*, vol. **21**, no. 4, pp. 630–645, 2017.

Nomura, H., Izawa, K., Ujiie, Y., Sato, J., Marutani, Y., Kono, M., and Kawasaki, H., An Experimental Study on Flame Propagation in Lean Fuel Droplet-Vapor-Air Mixtures by using Microgravity Conditions, *Symp. (Int.) Combust.*, vol. **27**, pp. 2667–2674, 1998.

Perona, P. and Malik, J., Scale Space and Edge Detection using Anisotropic Diffusion, *IEEE Trans. Pattern Anal. Mach. Intell.*, vol. **12**, no. 7, pp. 629–639, 1990.

Poinsot, T. and Veynante, D., *Theoretical and Numerical Combustion*, 2nd ed., Philadelphia, PA: R.T. Edwards Inc., 2005.

Pukelsheim, F., The Three Sigma Rule, *Am. Stat.*, vol. **48**, no. 2, pp. 88–91, 1994.

Sinnott, R., Virtues of the Haversine, *Sky and Telescope*, vol. **68**, no. 2, p. 159, 1984.

Spalding, D.B., *Some Fundamentals of Combustion*, vol. **2**, Cambridge, MA: Academic Press, 1955.

Sun, Z.Y., Liu, F.S., Bao, X.C., and Liu, X.H., Research on Cellular Instabilities in Outwardly Propagating Spherical Hydrogen-Air Flames, *Int. J. Hydrogen Energy*, vol. **37**, no. 9, pp. 7889–7899, 2012.

Thimothée, R., Caractérisation de la Propagation d'une Flamme dans un Milieu Diphasique (Brouillards) en Microgravité, PhD, Université d'Orléans, France, 2017.

Thimothée, R., Chauveau, C., Halter, F., and Gökalp, I., Characterization of Cellular Instabilities of a Flame Propagating in an Aerosol, *Proc. ASME Turbo Expo.*, vol. **4B**, pp. 1–11, 2015.

Thimothée, R., Chauveau, C., Halter, F., and Gökalp, I., Experimental Investigation of the Mechanisms of Cellular Instabilities Developing on Spherical Two-Phase Flames, *Combust. Sci. Technol.*, vol. **188**, nos. 11-12, pp. 2026–2043, 2016.

Thimothée, R., Chauveau, C., Halter, F., Nicoli, C., Haldenwang, P., and Denet, B., Microgravity Experiments and Numerical Studies on Ethanol/Air Spray Flames, *C. R. Mech.*, vol. **345**, no. 1, pp. 99–116, 2017.

Wilson, J.G., *The Principles of Cloud-Chamber Technique*, Cambridge, England: Cambridge University Press, 1951.